

Nitrogen-doped carbon foams synthesized from banana peel and zinc complex template for adsorption of CO₂, CH₄ and N₂

Arash Arami-Niya, Thomas E. Rufford and Zhonghua Zhu*

School of Chemical Engineering, The University of Queensland, St Lucia 4072 Australia

*Corresponding author: t.rufford@uq.edu.au

Keywords Carbon foam, biomass wastes, nitrogen doping, gas separation, CO₂ capture.

Abstract

We report nitrogen-doped and activated carbon foams with large specific surface areas prepared from banana peels using a self-template method with zinc nitrate, 2-aminophenol and furfural involved. Importantly, for development of these carbon foams for adsorption applications, we have extended the methodology of using the zinc complex template to investigate the effects of carbonization temperature, post-carbonization CO₂ activation and the N-content of the carbon foam on adsorption capacities for CO₂, CH₄ and N₂. The carbon foams produced contain up to 6.0 % wt nitrogen, and feature cellular macroporous structures with BET specific surface areas up to 1426 m².g⁻¹. The potential of the carbon foams for CO₂/N₂, CO₂/CH₄ and CH₄/N₂ separations was evaluated by measurement of pure fluid adsorption capacities using a gravimetric adsorption

apparatus. The adsorption capacities at a maximum pressure of 4000 kPa and 298 K were CO₂ 9.21 mmol.g⁻¹, CH₄ 5.29 mmol.g⁻¹ and N₂ 3.29 mmol.g⁻¹.

1 Introduction

Carbon foams with high void volumes, hierarchical porous structures, low bulk density, and good thermal and electrical conductivity have been reported for a range of significant applications including catalyst supports, energy storage electrodes, insulation and adsorption applications^{2, 3}. Carbon foams can be prepared from coal tar pitch and petroleum pitch^{4, 5}, polymeric precursors⁶ or renewable biomass-based precursors such as sucrose⁷ and banana peel¹. Renewable biomass materials for carbon foams may offer long-term environmental and economic advantages to fossil-fuel sources such as pitch, plus biomass materials can provide interesting natural macroporous structures that can be utilised to create novel foam properties.

Banana peel (BP) is an agricultural waste available in large volumes as bananas are a very popular and nutritionally important fruit for a wide population of the world - the global production of bananas is more than 100 million tonnes annually⁸. Our collective appetite for bananas generates a large volume of waste banana peels as the peel typically represents 30 - 40- % of the banana's weight^{9, 10} and, as an alternative to disposal of banana peels from industrial food processing plants to landfills, the banana peel has potential for utilisation in biogas generation¹¹, a source of aromatic compounds¹⁰ and activated carbon adsorbents^{12, 13}. Banana peels contain a diverse mix of biopolymers including pectin, hemicellulose, cellulose, and lignin^{9, 14}. Of particular relevance to our current work on carbon foams are the gel-forming properties of BP-pectins⁹ and the polar surface functional groups on various BP compounds,

which can act as sites for metal ion complexation (often cited for use in heavy metal ion adsorption^{15, 16}).

Lv et al.¹ utilised both BP's gel-forming properties and metal-complexation sites to adsorb phenolic resin-precursors to produce self-templated hierarchical carbon foams for supercapacitor electrodes. In this procedure, the introduction of 2-aminophenol to the carbon provides nitrogen-containing functional groups on the carbon foam that may present attractive properties for supercapacitor electrodes (as evaluated by Lv et al.¹) and enhanced CO₂ adsorption. In this study, we extend the self-templated carbon foam methodology of Lv et al.¹, and others^{17, 18} by switching the argon gas to CO₂ at the carbonization temperature, and the effects of carbonization temperature, post-carbonization CO₂ activation and the N-content of the carbon foam on adsorption capacities for CO₂, CH₄ and N₂ have been comprehensively investigated.

2 Experimental methods

2.1 Materials

Queensland-grown yellow Cavendish bananas (*Musa acuminata*) were purchased from a local supermarket in Brisbane. After the first author ate the fruit, the banana peels (BP) were washed in distilled water, dried in air overnight and sliced into small pieces. Reagent grade zinc nitrate hexahydrate (Zn(NO₃)₂·6H₂O), furfural (C₅H₄O₂) and 2-aminophenol (C₆H₇NO) were used without further purification. The purities of gases used in this work, as stated by the supplier Coregas Australia, were 99.999 % for helium, argon and nitrogen, and 99.995 % for carbon dioxide and methane.

2.2 Preparation of nitrogen-doped carbon foams

The procedure to prepare carbon foams was based on the self-template method proposed by Lv et al.¹ using zinc ions coordinated with carboxylic and hydroxyl groups on the BP's pore surfaces. The key process steps in this procedure, as summarised in Fig. 1, were (1) The BP particles were soaked in 2 mol.L⁻¹ zinc nitrate solution at 343 K in a closed vessel for 7 days to form zinc complexes. (2) The reaction vessel was opened and the excess water was evaporated over 14 days at 333 K to obtain brown zinc complexes. (3) The zinc complexes were soaked in a mixture of furfural and 2-aminophenol at 343 K for 7 days. This step produces a slurry of banana peel zinc complexes impregnated with a 2-aminophenol-furfural resin, which subsequently provides a N-rich carbon source during pyrolysis. (4) 7 g of the slurry was pressed by hand into a cylindrical quartz crucible (2.54 cm diameter × 2.54 cm height), dried at 393 K overnight and carbonized in a horizontal tube furnace at temperatures in the range of (1023 – 1273) K for carbonisation times of 1 to 11 hrs. In addition, we extended Lv et al.'s procedures¹ to produce a set of CO₂ activated carbon foams by switching the gas flow from argon to CO₂ once the carbonisation temperature had been reached. The heating rate in all experiments was 10 K.min⁻¹. Carbons produced from the banana peel zinc complexes are labelled as chemically-modified banana foams CBF-T-FF-t, where T = [1023 - 1273] K, FF is the gas atmosphere and t the duration of the carbonisation step.

As a comparison, we also prepared carbons by direct pyrolysis of the sliced BP in argon at 873 K to produce BP-char (heating rate = 10 K min⁻¹; hold time = 1 hr) and by CO₂ activation of this char to produce activated BP carbons (BPAC). The CO₂ activation was performed after the char had cooled in argon, and then the gas was switched to 50 mL.min⁻¹ CO₂ and the furnace

temperature increased again at 10 K min⁻¹ to 1023 K for 1 or 3 hours. These samples were labelled BPAC followed by the activation temperature, gas type and activation duration.

The yield of each carbon product in the pyrolysis or pyrolysis plus carbonization steps was calculated as:

$$Yield(\%) = \left(\frac{W_f}{W_i}\right) \times 100 \quad (1)$$

where W_i and W_f are the dry weight (g) of feed for each process (BP, BP char or impregnated BP) and dry weight (g) of products (bio-char, BPACs or CBFs), respectively.

2.3 Characterizations

The carbons were characterized by scanning electron microscopy (SEM, JEOL JSM-6100), thermogravimetric analysis (TGA, Perkin Elmer STA 6000) and X-ray photoelectron spectroscopy (XPS, Kratos Axis ULTRA X-ray photoelectron spectrometer using a monochromated Al K α (1486.6 eV) excitation source). The quantitative analysis of XPS data was performed with CasaXPS software after Shirley background subtraction. Bulk concentrations of C, H and N were determined with an Elemental Analyzer (FlashEA1112 series), and the O concentrations were assumed to be the residual between 100 % and the sum of C, H and N concentrations.

Pore textural properties of the carbon foams were characterised by mercury intrusion porosimetry (MIP) measured at pressure of (20 – 414000) kPa (Micromeritics PoreSizer 9320) and sorption analyses with CO₂ at 273 K and 303 K as well as N₂ at 77 K (Micromeritics TriStar II 3020). Samples were degassed at 473 K and a pressure of 10⁻⁵ torr for 24 hr prior to CO₂ and N₂ sorption measurements. Specific surface areas (S_{BET}) were calculated by the Brunauer-

Emmett-Teller method at the relative pressures in the range of $P/P_0 = 0.05 - 0.30$; total pore volumes were estimated at $P/P_0 = 0.98$; and volumes of micropores were calculated from both the 77 K N_2 and 273 K CO_2 isotherms using the Dubinin-Astakhov (D-A) equation.^{19,20} The micropore surface area was calculated using Dubinin-Radushkevich (D-R) equation on the CO_2 adsorption data at 273 K. The pore size distributions (PSD) were determined using a density functional theory model (DFT) algorithm for carbon slit pores supplied with the Micromeritics instrument.

2.4 Gravimetric adsorption equilibria measurement

Adsorption isotherms of pure fluids CO_2 , CH_4 , and N_2 on carbons were measured at (298, 313 and 323) K and pressures up to 4000 kPa using a BELSORP-BG instrument (BEL Japan) equipped with a RUBOTHERM magnetic floating balance. Prior to adsorption measurements the carbon foam was degassed in-situ at 473 K for 24 hrs. We have previously described elsewhere the operation of this apparatus to measure adsorption on carbon materials¹⁹, so we only include here in the supporting information a brief description of the BELSORP-BG measurement procedures.

3 Results and discussions

3.1 Preparation of chemically modified banana peel foam monoliths

The SEM images in Fig. 2 show the morphology of the banana peel with open cell structures that are approximately 5 – 20 μm wide and coated in biopolymers. The total nitrogen concentration of the raw BP determined by CHNS Elemental Analyser was 1.9 %wt (Table 1), which is comparable to the BP nitrogen concentrations reported in other studies¹⁴. Proximate analysis of the raw BP by thermal gravimetric analysis obtained 67.7 %wt volatiles, 24.2 %wt fixed carbon

and 8.2 %wt ash. The dried (samples were dried at 473 K under nitrogen) raw BP's residual mass after the TGA measurement shown in Fig. 3 is consistent with the yield of 38.8 %wt BP-char produced by pyrolysis of raw BP in the tube furnace (Table 1).

The TGA weight loss curve in Fig. 3 of the banana peel treated with zinc nitrate and impregnated with the furfural + 2-aminophenol resin (dry basis) shows that the BPC composite has a greater thermal stability than the raw BP at temperatures in the range (500 -773 K); this BPC weight loss curve is consistent with the decomposition of aminophenol-furfural resins reported in the literature. For example, Patel et al. ²⁰report aminophenol-furfural resins will soften at temperatures above 473 K and then harden at temperatures from 703-843 K due to devolatilization of the resin and BP polymers. The BPC weight loss observed in Fig. 3 at temperature above 1100 K includes the evaporation of zinc via reduction of ZnO (derived from the zinc nitrate) to metallic zinc ^{21, 22}. The EDX analysis of BPC and carbon foams CBF-1023-Ar-3h and CBF-1273-Ar-3h (see Fig. S2) confirms the loss of zinc from the composite after pyrolysis at 1273 K. Table 1 shows the yields of CBFs produced in argon ranged from 65.7 %wt to 23.6 %wt; the yield decreased at higher temperatures and longer carbonisation time.

An aim of this study was to produce monolithic carbon foams with a mechanically stable, open cellular structure and the chemically-modified banana foam synthesis method successfully produced monoliths of CBF, as summarised in Table 1. The inset photograph for CBFs in Fig. 1 shows a typical example of a CBF monolith in the shape of the crucible mould. In contrast, BPAC-1023-CO₂-1h produced by a more conventional carbonisation and CO₂ activation process was a loose agglomeration of granules that was easily crumbled by hand, thus not as strong and uniform as the CBFs. The SEM images of CBF-1273-Ar-3h in Fig. 4a-c show a highly porous

foam-like open cell structure with typical carbon foam features of ligaments and walls^{23, 24}. Clearly, the texture of the CBF sample is different to the texture of the BPAC-1023-CO₂-1h produced by CO₂ activation of BP (Fig. 4g-i). Mercury intrusion porosimetry (Fig. 5) shows a broad distribution of macroporous channels in CBF-1273-Ar-3h, the largest channels are approximately 80 µm wide. Table 2 provides a summary of the microporous textural properties of the CBFs and these results are discussed in details in later sections.

The CO₂ activation of BP alone does not produce the carbon foam structure, we can infer that the porous structure developed in the CBF results partly from the devolatilisation and polymerisation of furfural-aminophenol resin. There are three key stages in such a bubble growth foaming process, as has been described by Beecham et al.²⁵: firstly, the resin melts around 473 K, secondly as the temperature increases further light hydrocarbons such as unreacted furfural evolve from the resin, and thirdly polymerisation of the resin leads to additional evolution of gas products and increase in the viscosity of the resin. Finally, at temperatures between 703 -843 K the molten resin has reacted to such a degree that the resin solidifies. In the presence of the BP-zinc nitrate complex, the biopolymers of the BP which are mostly released from raw BP at temperatures below 673 K (Fig. 3) may provide additional gas for bubble formation and growth in the resin phase.

The bulk nitrogen concentration of CBF-1023-Ar-3h was 6.0 %wt (Table 1), 2.6 times the nitrogen content of the activated carbon BPAC-1023-CO₂-1h (2.3 %wt N). The source of the additional N in the chemically-modified CBF is the 2-aminophenol (C₆H₇NO contains 12.83 %wt N) and the intermediate composite BPC contained 8.0 %wt N. Characterisation of the N-containing groups in BPC by XPS (as shown in Fig. 6a and Table 3) confirms the presence of

amine groups (N-1 at binding energy (BE) of 399.4 ± 0.1 eV)²⁶⁻²⁸ and amides (N-2 at BE = 400.5 ± 0.1 eV) from the 2-aminophenol-furfural resin²⁰. The N-3 group detected in the XPS of BPC around BE = 407.3 ± 0.1 eV may be attributed to unreacted nitrate salts from the zinc nitrate reagent.²⁶⁻²⁹

Carbonisation at higher temperature (1273 K) and longer duration (8 h and 11 h) decomposed some N-functional groups on the carbon surface to reduce total N concentrations in the CBFs to 4.6 -3.9 %wt. The XPS data for CBF-1273-Ar-3h in Fig. 6b and Table 3 show that after carbonisation at 1273 K the nitrogen from 2-aminophenol is converted to pyridinic-N (N-4, BE = 398.2 ± 0.1 eV), pyrrolic/pyridone-N (N-5, BE = 399.8 ± 0.1 eV), and quaternary-N (N-6, BE = 401.1 ± 0.1 eV) structures.^{30, 31} These results are consistent with other reports on the carbonization of N-rich precursors to introduce nitrogen to carbon frameworks.³²⁻³⁴ For example, at temperature above 873 K pyridinic and pyrrolic structures are produced by decomposition of amide groups³⁵ and the reaction of NO₃ with carbon; and Chambrion et al.³⁰ proposed C-NO reactions that lead to quaternary-N.

3.2 Development of microporosity in the carbon foams

N₂ sorption isotherms were measured at 77 K on the BPAC-1023-CO₂-1h and CBFs and are shown in Fig. 7a. A summary of pore structure properties is provided in Table 2. The N₂ sorption isotherm on BP-char was not successful, which suggests a low degree of activation and lack of pore development³⁶. The micropore volume and D-R specific surface area of the BP-char determined from the 273 K CO₂ sorption isotherms were $0.14 \text{ cm}^3 \text{ g}^{-1}$ and $391.1 \text{ m}^2 \text{ g}^{-1}$, respectively. The activated carbon BPAC-1023-CO₂-1h produced by conventional pyrolysis and CO₂ activation exhibited a Type IV isotherm³⁶ with a hysteresis loop at relative pressures P/P₀

around 0.8 that suggests the larger mesopores are open and tubular shaped (type A hysteresis). In addition, the shape of the isotherm at lower P/P_0 suggests there are slit shaped pores (type B hysteresis)³⁷. The pores size distribution in Fig. 7b shows BPAC-1023-CO₂-1h has a bimodal distribution of micropores around 13 Å and small mesopores around 20 – 25 Å.

The N₂ isotherms of the CBFs prepared under argon also feature hysteresis loops that suggest the presence of mesopores together with a degree of microporosity. As indicated by the uptake of N₂ at 77 K (Fig. 7a) and calculated D-R micropore N₂ accessible surface areas the microporosity of CBFs prepared under argon increased almost two-fold at the higher carbonization temperature, and prolonged carbonisation times produced a further increase in micropore surface area of about 15 % (D-R micropore surface area). The CO₂ isotherms measured at 273 K (Fig. 8a), and pore texture parameters in Table 2 derived from these isotherms, show consistent trends for micropore development in the CBFs as the N₂ sorption analyses. The evaporation of ZnO particles from the carbon structure is likely to be one reason for the greater volume of micropores produced at a carbonisation temperature of 1273 K. The CBF with the highest surface area prepared under argon (no CO₂ activation) was CBF-1273-Ar-11h with a BET surface area of 190.4 m².g⁻¹ and CO₂ D-R micropore surface area of 628.5 m².g⁻¹; however, the yield of this CBF was significantly lower than that of the CBFs prepared at 1023 K and short carbonisation times. The BET surface area of CBF-1273-Ar-11h is similar to that of activated carbon BPAC-1023-CO₂-1 (204.3 m².g⁻¹); but the CBFs have both larger N₂-accessible pore volumes and narrow micropore volumes as measured by CO₂ sorption (Table 2). Notably, the CBFs produced in this study have lower surface areas and pore volumes than the foams reported by Lv et al.¹. A possible explanation for the difference in the results could be the ratio of furfural-aminophenol resin to BP used in the soaking experiments and this synthesis detail was not included in Lv et al.'s

paper. To summarize, the results of our experiments with CBFs prepared in argon suggest (1) that the optimum carbonisation temperature to maximise surface area under argon is 1273 K, and (2) carbonisation at 1273 K for more than 3 h enhances micropore development but this additional porosity is obtained with a reduced product yield. The N₂ and CO₂ sorption isotherms on CBF-1023-CO₂-3h in Fig. 7 and Fig. 8 highlight the effectiveness of the CO₂ activation step to develop microporosity compared to carbonisation of the chemically modified BP-resin composite BPC under just argon. Even at a carbonisation temperature of 1023 K, the CO₂ activated CBF has a BET area of more than 350 m².g⁻¹ and twice the total pore volume as CBF-1023-Ar-3h (Table 2, from the N₂ 77 K isotherm). The CO₂ activation process acts to widen a broad range of pore sizes - as evidenced by the increase in macropore volume by MIP (Fig. 5) and the increase in pore volume for widths from 10 -40 Å determined from the N₂ sorption (Fig. 7b). Under CO₂ activation conditions, like in the case of argon-carbonized CBFs, the surface area and micropore volumes increase with the carbonisation temperature to a maximum BET area of 1426.1 m².g⁻¹ for CBF-1273-CO₂-1h. The yield of CBF-1273-CO₂-1h was 14.2 %wt so by this method there is a high yield penalty to produce the highest surface area CBF. We attempted to produce a CO₂ activated CBF at 1273 K treated in CO₂ for 3 h (i.e. CBF-1273-CO₂-3h) but this activation condition consumed almost all the carbon and there was insufficient product recovered from the furnace to characterize.

3.3 Adsorption equilibria of pure gases

The CO₂ adsorption capacities of the CBFs and BPAC measured on the Tristar II at 273K and 303 K and pressures up to 130 kPa are shown in Fig. 8a and Fig. 9. The carbon with the highest capacity for CO₂ at these conditions was CBF-1273-CO₂-1h (5.75 mmol.g⁻¹ at 273 K), that is the

sample with the highest surface area and micropore volume. Compared to other carbon foams reported on literature, CBFs exhibited a higher capacity for CO₂ per micropore surface area than some other carbon foams reported in the literature - for example at 273 K, Tsyntsarki et al.³⁹ reported 3.35 mmol.g⁻¹ CO₂ on a pitch-derived and steam activated foam with BET of 933 m².g⁻¹ and Liu et al.¹⁷ reported 2.35 mmol.g⁻¹ CO₂ on nitrogen-doped porous carbons with a surface area of a 1148 m².g⁻¹. This second example was prepared from banana peels using an aluminium nitrate synthesis procedure similar to the zinc nitrate method we used.

Fig. 10 provides a clearer picture of the effect of nitrogen functional groups and micropore surface area on CO₂ uptake on the CBFs. CBP-1023-Ar-3h has the highest CO₂ capture per micropore surface area, which confirms the important effect of nitrogen functional groups on the surface of the CBFs. In addition, almost linear effect of porosity development on the adsorption of CO₂ is noticeable in Fig. 10b. The value of CO₂ uptake divided by micropore surface area of the CBFs (Fig. 10a) is higher than almost all the biomass based activated carbons and nitrogen-modified activated carbons reported on the recent review by Rashidi and Yusup³⁸. CO₂ adsorption analysis of the CBFs at 303 K (Fig. 9) showed BPAC-1023-CO₂-1h with the lowest micropore surface area and nitrogen contents obtained the lowest and CBF-1273-CO₂-1h with the highest measured micropore surface area and 4.2% nitrogen content the highest CO₂ capture.

Based on the high CO₂ uptakes measured at low pressure, we selected CBF-1273-CO₂-1h for the high-pressure adsorption measurements. Fig. 11**Error! Reference source not found.**a to Fig. 13**Error! Reference source not found.**a present the absolute adsorption capacities for CO₂, CH₄ and N₂ measured with the BelSORP apparatus CBF-1273-CO₂-1h at temperatures of (298, 313 and 323) K. The high-pressure adsorption equilibria data is also included in Table S 1 of the

Supporting Information. Compared to the CO₂, CH₄ and N₂ adsorption capacities of other carbon adsorbents reported in the literature, BPAC-1023-CO₂-1h has a reasonable capacity for these gases⁴⁰⁻⁴².

The absolute adsorption capacities of CO₂, CH₄ and N₂ at 298 K on CBF-were also measured on CBF-1273-Ar-3h (Fig. 14**Error! Reference source not found.** and Table S 2). As expected, the adsorption capacities on the carbon foam prepared under argon were lower than the capacities on the CO₂ activated carbon foam CBF-1273-CO₂-1h. The adsorption capacities for CO₂, CH₄ and N₂ on CBF-1273-CO₂-1h measured at 298 K and 4000 KPa were about 63 %, 76 % and 34% higher, respectively, than the capacities on CBF-1273-Ar-3h. This comparative results highlights that the CO₂ activation of the foam has improved the selectivity of the CBF for CO₂ and CH₄ over N₂.

A temperature-dependent, semi-empirical Toth isotherm model was tested to determine the ability of CBF-1273-CO₂-1h to allow the prediction adsorption capacities of CO₂, CH₄ and N₂ across the range of pressure and temperature conditions measured in this study. The Toth isotherm model is described by Equation 2⁴³:

$$Q_{\mu i}^{Toth} = Q_{\mu si}^{Toth} \frac{b_i P}{[1 + (b_i P)^{t_i}]^{1/t_i}} \text{ with } b_i = b_{o,i} \exp\left(\frac{-\Delta H_{Toth,i}}{RT}\right) \quad (2)$$

where R is the molar gas constant, P and T are the measurement pressure and temperature. In the regression of this model, $\Delta H_{Toth,i}$ was treated as an adjustable parameter together with the empirical parameters ($Q_{\mu si}^{calc}$, $b_{o,i}$ or t_i). The parameters t_i is used to characterise the heterogeneity of the adsorption sites in the model, but it was treated as adjustable parameter in the regression. The best fit parameters of Equation 2 were determined using a least-squares regression analysis

to minimize the standard deviation (SD) between the measured capacities, Q_{μ} , and the capacities Q_{μ}^{calc} calculated with the model ($SD = ((1/N)\sum(Q_{\mu}^{meas} - Q_{\mu}^{calc})^2)^{1/2}$ where N is the number of data points regressed).

Table 4 lists the optimized parameters of Equation 2 and the standard deviations (SD) resulting from the regression of the Toth model to the CBF-1273-CO₂-1h high pressure adsorption data. Deviations ($Q_{\mu}^{meas} - Q_{\mu}^{calc}$) between the measured and the calculated capacities of Toth model that are shown in Fig. 11**Error! Reference source not found.**, Fig. 12 b and Fig. 13**Error! Reference source not found.** are in the range of ± 0.1 at most of the pressure points. This isotherm model has a SD of 0.06 mmol.g⁻¹ for CO₂, 0.03 mmol.g⁻¹ for CH₄ and 0.009 mmol.g⁻¹ for N₂.

4 Conclusions

Monolithic carbon foams with an open cellular structure were successfully produced from the chemically-modified banana peel precursor. The evaporation of zinc ions, which were introduced into the BP surface to form metal complexes as templates in its structure, from the carbon structure at a carbonisation temperature of 1273 K was showed to be one reason for the greater volume of micropores produced. The CO₂ activation process was found more effective in development of micro- and macroporosity compared to the carbonisation of the chemically modified BP-resin composite BPC under just argon. After carbonisation of the precursors at 1273 K the nitrogen from 2-aminophenol and any naturally occurring N in the banana peel was converted to pyridinic-N, pyrrolic/pyridone-N, and quaternary-N structures. The presence of N in the carbon foam produces enhanced the CO₂ adsorption capacity of the carbon foams. Micropore

development and nitrogen functionalities had positive effects on the CO₂ uptake capacity of the carbon foams. The carbon foam CBF-1273-CO₂-1h with the highest CO₂ and CH₄ adsorption capacities and the most promising CO₂/N₂ equilibrium selectivity are comparable to adsorbents reported in literature.

Acknowledgements

This research was funded by the Australian Research Council (DE140100569, FT120100720) with additional scholarship support for Mr Arami-Niya provided through a UQ International Postgraduate Research Scholarship. We thank Dr Ge Lei for technical assistance in the laboratory, Miss Yangyang Wen for assistance with the CHNS measurements and Dr Barry Wood for assistance with XPS. We acknowledge the facilities and technical assistance of the Australian Microscopy & Microanalysis Research facility at the Centre for Microscopy & Microanalysis at the University of Queensland.

Appendix A. Supplementary data

Supplementary data related to this article includes: a description of the gravimetric adsorption apparatus, SEM images of dry banana peel and banan peel char, EDX spectra, and tabulated high pressure adsorption data.

References

1. Y. Lv, L. Gan, M. Liu, W. Xiong, Z. Xu, D. Zhu and D. S. Wright, *Journal of Power Sources*, 2012, **209**, 152-157.
2. M. Inagaki, F. Kang, M. Toyoda and H. Konno, in *Advanced Materials Science and Engineering of Carbon*, eds. M. Inagaki, F. Kang, M. Toyoda and H. Konno, Butterworth-Heinemann, Boston, 2014, pp. 189-214.
3. H. D. Asfaw, M. Roberts, R. Younesi and K. Edstrom, *Journal of Materials Chemistry A*, 2013, **1**, 13750-13758.
4. C. Chen, E. B. Kennel, A. H. Stiller, P. G. Stansberry and J. W. Zondlo, *Carbon*, 2006, **44**, 1535-1543.
5. G.-P. Hao, W.-C. Li, D. Qian, G.-H. Wang, W.-P. Zhang, T. Zhang, A.-Q. Wang, F. Schüth, H.-J. Bongard and A.-H. Lu, *Journal of the American Chemical Society*, 2011, **133**, 11378-11388.
6. M. Inagaki, T. Morishita, A. Kuno, T. Kito, M. Hirano, T. Suwa and K. Kusakawa, *Carbon*, 2004, **42**, 497-502.
7. R. Narasimman and K. Prabhakaran, *Carbon*, 2012, **50**, 1999-2009.
8. Food and Agriculture Organization of the United Nations, FOASTAT, <http://faostat3.fao.org/home/E>.
9. T. H. Emaga, C. Robert, S. N. Ronkart, B. Wathelet and M. Paquot, *Bioresource Technology*, 2008, **99**, 4346-4354.
10. L. Ji and G. Srzednicki, in *Acta Horticulturae*, 2015, pp. 541-546.
11. W. P. Clarke, P. Radnidge, T. E. Lai, P. D. Jensen and M. T. Hardin, *Waste Management*, 2008, **28**, 527-533.

12. H. Gupta and B. Gupta, *Desalination and Water Treatment*, 2016, **57**, 9498-9509.
13. J. Ma, D. Huang, J. Zou, L. Li, Y. Kong and S. Komarneni, *Journal of Porous Materials*, 2015, **22**, 301-311.
14. R. Jiang, S. Sun, Y. Xu, X. Qiu, J. Yang and X. Li, *Water Science and Technology*, 2015, **71**, 1458-1462.
15. J. R. Memon, S. Q. Memon, M. I. Bhangar, A. El-Turki, K. R. Hallam and G. C. Allen, *Colloids and Surfaces B: Biointerfaces*, 2009, **70**, 232-237.
16. M. Thirumavalavan, Y.-L. Lai, L.-C. Lin and J.-F. Lee, *Journal of Chemical & Engineering Data*, 2009, **55**, 1186-1192.
17. R.-L. Liu, W.-J. Ji, T. He, Z.-Q. Zhang, J. Zhang and F.-Q. Dang, *Carbon*, 2014, **76**, 84-95.
18. E. M. Lotfabad, J. Ding, K. Cui, A. Kohandehghan, W. P. Kalisvaart, M. Hazelton and D. Mitlin, *ACS Nano*, 2014, **8**, 7115-7129.
19. A. Arami-Niya, T. E. Rufford and Z. Zhu, *Carbon*, 2016, **103**, 115-124.
20. P. S. Patel and S. R. Patel, *European Polymer Journal*, 1987, **23**, 733-735.
21. B. Liu, H. Shioyama, T. Akita and Q. Xu, *Journal of the American Chemical Society*, 2008, **130**, 5390-5391.
22. B. Liu, H. Shioyama, H. Jiang, X. Zhang and Q. Xu, *Carbon*, 2010, **48**, 456-463.
23. R. Kumar, S. R. Dhakate, T. Gupta, P. Saini, B. P. Singh and R. B. Mathur, *Journal of Materials Chemistry A*, 2013, **1**, 5727-5735.
24. M. Inagaki, J. Qiu and Q. Guo, *Carbon*, 2015, **87**, 128-152.
25. T. Beechem, K. Lafdi and A. Elgafy, *Carbon*, 2005, **43**, 1055-1064.

26. N. Graf, E. Yegen, T. Gross, A. Lippitz, W. Weigel, S. Krakert, A. Terfort and W. E. S. Unger, *Surface Science*, 2009, **603**, 2849-2860.
27. R. J. J. Jansen and H. van Bekkum, *Carbon*, 1995, **33**, 1021-1027.
28. J. R. Pels, F. Kapteijn, J. A. Moulijn, Q. Zhu and K. M. Thomas, *Carbon*, 1995, **33**, 1641-1653.
29. A. Krepelova, J. Newberg, T. Huthwelker, H. Bluhm and M. Ammann, *Physical Chemistry Chemical Physics*, 2010, **12**, 8870-8880.
30. P. Chambrion, T. Suzuki, Z.-G. Zhang, T. Kyotani and A. Tomita, *Energy & Fuels*, 1997, **11**, 681-685.
31. H. Chen, G. Lin, Y. Chen, W. Chen and H. Yang, *Energy & Fuels*, 2015.
32. G.-P. Hao, W.-C. Li, D. Qian and A.-H. Lu, *Advanced Materials*, 2010, **22**, 853-857.
33. J. P. McGann, M. Zhong, E. K. Kim, S. Natesakhawat, M. Jaroniec, J. F. Whitacre, K. Matyjaszewski and T. Kowalewski, *Macromolecular Chemistry and Physics*, 2012, **213**, 1078-1090.
34. D. Hulicova-Jurcakova, M. Kodama, S. Shiraiishi, H. Hatori, Z. H. Zhu and G. Q. Lu, *Advanced Functional Materials*, 2009, **19**, 1800-1809.
35. R. J. J. Jansen and H. van Bekkum, *Carbon*, 1994, **32**, 1507-1516.
36. H. Marsh and F. Rodríguez-Reinoso, in *Activated Carbon*, eds. H. Marsh and F. Rodríguez-Reinoso, Elsevier Science Ltd, Oxford, 2006, pp. 143-242.
37. D. D. Duong, in *Adsorption Analysis: Equilibria and Kinetics*, Imperial College Press, 1998, pp. 49-148.
38. N. A. Rashidi and S. Yusup, *Journal of CO2 Utilization*, 2016, **13**, 1-16.

39. B. Tsyntsarski, B. Petrova, T. Budinova, N. Petrov, L. F. Velasco, J. B. Parra and C. O. Ania, *Microporous and Mesoporous Materials*, 2012, **154**, 56-61.
40. S. García, J. J. Pis, F. Rubiera and C. Pevida, *Langmuir*, 2013, **29**, 6042-6052.
41. F. Dreisbach, R. Staudt and J. U. Keller, *Adsorption*, 1999, **5**, 215-227.
42. T. E. Rufford, G. C. Y. Watson, T. L. Saleman, P. S. Hofman, N. K. Jensen and E. F. May, *Industrial & Engineering Chemistry Research*, 2013, **52**, 14270-14281.
43. J. Toth, *Acta Chim. Acad. Sci. Hung.*, 1971, **69**, 311-328.

Figure captions

Fig. 1 Process block flow diagram of (a) zinc complex templated furfural + 2-aminophenol procedures to produce activated carbons and (b) pyrolysis to char, and then physical activation with CO₂.

Fig. 2 SEM images of dry peel from Cavendish bananas (BP).

Fig. 3 Thermal gravimetric analysis of dried banana peel (BP) and banana peel-zinc composite impregnated with furfural and 2-aminophenol (BPC) in 20 mL/min N₂, heating rate 10 K/min. Weight % is on a dry basis after removal of adsorbed moisture and any other light gases at temperature below to 473 K.

Fig. 4 SEM images of soft templated carbon foams (a-c) BPC- 1273-Ar-3h, prepared at 1273 K under argon for 3 hours and (d-f) BPC- 1273-CO₂-1h, prepared at 1273 K under CO₂ for 1 h, and (g-i) example of a CO₂ activated banana peel carbon ACBP-1023-CO₂-1h.

Fig. 5 Differential pore volumes versus pore diameter obtained from mercury intrusion porosimetry for BPC-1273-Ar-3h and BPC-1273-CO₂-1h.

Fig. 6 XPS spectrum of BPC, BPC-1273-Ar-3h and BPC-1273-CO₂-1h and high-resolution fitted XPS spectra of N 1s peak for these samples.

Fig. 7 (a) N₂ adsorption-desorption isotherm measured at 77 K on on CO₂ activated banana peel carbon ACBP-1023-CO₂-1. And the zinc-complex furfural + 2-aminophenol derived banana peel carbons (BPCs). (b) Pore size distribution determined from isotherms measured at 77 K with N₂.

Fig. 8 (a) CO₂ adsorption capacities at 273 K for banana peel derived zinc-complex templated carbon foams and activated carbons measured at pressures up to 130 kPa on the Micromeritics Tristar II (b) Pore size distribution determined from isotherms measured at 273 K with CO₂.

Fig. 9 CO₂ adsorption capacities at 303 K for chemically-modified banana foams and activated carbons measured at pressures up to 130 kPa on the Micromeritics Tristar II.

Fig. 10 Relationship between the CO₂ uptake capacity and (a) nitrogen content, (b) micropore surface area.

Fig. 11 Measured and modelled CO₂ adsorption capacities for soft templated carbon foam BPC-1273-CO₂-1h at temperatures of 298 K, 313 K and 323 K. (a) Absolute adsorption capacities. The lines represent the predictions of the Toth model (Eq. 4). (b) Deviations between the measured and the calculated adsorption capacities.

Fig. 12 Measured and modelled CH₄ adsorption capacities for soft templated carbon foam BPC-1273-CO₂-1h at temperatures of 298 K, 313 K and 323 K. (a) Absolute adsorption capacities. The lines represent the predictions of the Toth model (Eq. 4). (b) Deviations between the measured and the calculated adsorption capacities.

Fig. 13 Measured and modelled N₂ adsorption capacities for soft templated carbon foam BPC-1273-CO₂-1h at temperatures of 298 K, 313 K and 323 K. (a) Absolute adsorption capacities. The lines represent the predictions of the Toth model (Eq. 4). (b) Deviations between the measured and the calculated adsorption capacities.

Fig. 14 CO₂, CH₄ and N₂ absolute adsorption capacities at 298 K on BPC-1273-Ar-3h measured on the Belsorb-BG.

Table 1 Carbon product yield, proximate analysis by ASTM D 7582-10 using TGA and elemental composition measured by CHNS/O analyser.

Sample	Description of carbon form	Yield (%)	ASTM D 7582-10			Elemental Composition (%)		
			Fixed carbon (% wt)	Volatiles (% wt.)	Ash (% wt)	N	C	H
BP-Raw	-	-	24.2	67.7	8.2	1.9	42.0	5.6
BP-char	Agglomerated carbon particles	38.8	65.8	21.6	12.7	2.1	48.8	1.1
BPC	-	-	40.8	45.9	13.3	8.0	32.4	3.6
BPC-1023-Ar-3h	Monolith carbon	65.7	66.1	22.3	11.6	6.0	47.5	0.7
BPC-1273-Ar-3h	Monolith carbon	30.1	84.7	10.7	4.6	4.6	70.0	1.3
BPC-1273-Ar-8h	Monolith carbon	26.4	82.3	12.2	5.4	4.5	70.4	1.2
BPC-1273-Ar-11h	Monolith carbon	23.6	85.6	10.5	3.9	3.9	70.4	1.0
BPC-1023-CO ₂ -3h	Monolith carbon	45.2	55.8	32.3	11.9	3.9	27.4	1.1
BPC-1123-CO ₂ -3h	Monolith carbon	24.6	44.4	31.9	23.7	4.0	30.2	1.4
BPC-1273-CO ₂ -1h	Monolith carbon	14.2	76.3	16.2	7.5	4.2	43.5	2.2
BPAC-1023-CO ₂ -1h	Agglomerated carbon particles	67.9	60.1	28.6	11.3	2.3	33.8	1.5

Table 2 Surface textural properties of zinc complex templated carbon foams from banana peel (CBFs), BP-char and a CO₂ activated banana peel carbon (BPAC-1023-CO₂-1h) determined from sorption isotherms of N₂ at 77 K and CO₂ at 273 K.

Sample	N ₂				CO ₂	
	D-A Micropore Surface area (m ² ·g ⁻¹)	Micropore Volume (cm ³ ·g ⁻¹)	BET surface area (m ² ·g ⁻¹)	Pore volume (cm ³ ·g ⁻¹)	D-R Micropore Surface area (m ² ·g ⁻¹)	Micropore Volume (cm ³ ·g ⁻¹)
BP-char	-	-	-	-	391.1	0.14
BPC-1023-Ar-3h	102.7	0.04	91.5	0.093	337	0.14
BPC-1273-Ar-3h	198.3	0.07	169	0.18	620.9	0.29
BPC-1273-Ar-8h	225.7	0.08	183.6	0.19	675.5	0.31
BPC-1273-Ar-11h	228.7	0.08	190.4	0.17	628.5	0.3
BPC-1023-CO ₂ -3h	446.7	0.16	352.2	0.22	369.3	0.23
BPC-1123-CO ₂ -3h	644.7	0.26	533.6	0.31	365.3	0.35
BPC-1273-CO ₂ -1h	1611	0.56	1426.1	0.83	881.93	1.09
BPAC-1023-CO ₂ -1h	234.1	0.11	204.3	0.11	299.9	0.27

Table 3 Nitrogen contents, peak analysis and type of nitrogen groups on the BPC and carbon foam surfaces determined using XPS; N-1: primary amine groups, N-2: amide groups, N-3: nitrates, N-4: pyridine, N-5: pyrrol or other forms of pyridine like nitrogens, N-6: quaternary nitrogen.

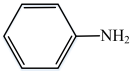
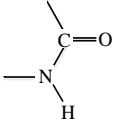
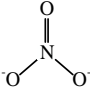
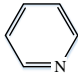
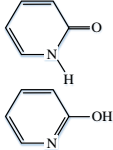
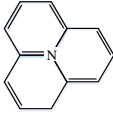
Sample	Overall N content (%)	Overall O content (%)	N-1 (%)	N-2 (%)	N-3 (%)	N-4 (%)	N-5 (%)	N-6 (%)
			399.4 ± 0.1 eV	400.5 ± 0.1 eV	407.3 ± 0.1 eV	398.2 ± 0.1 eV	399.8 ± 0.1 eV	401.1 ± 0.1 eV
			Schematic					
								
BPC	20.6	6.9	36.9	21.6	41.5	-	-	-
BPC-1273-Ar-3h	7.5	4.6	-	-	-	37.8	17.9	44.3
BPC-1273-CO ₂ -1h	10	4.9	-	-	-	38.7	37.2	24.1

Table 4 Fitting parameters of the Toth Model for CO₂, CH₄ and N₂ on CBF-1273-CO₂-1h

Gas	Toth model				
	$Q_{max,i}$ ($mmol \cdot g^{-1}$)	$b_{0,i} \cdot 10^6$ (MPa)	$-\Delta H_{Toth,i}$ ($J \cdot mmol^{-1}$)	t_i	SD ($mmol \cdot g^{-1}$)
CO ₂	24.7	0.22	30	0.26	0.21
CH ₄	7.65	0.64	20.3	0.61	0.04
N ₂	5.75	1.24	15.7	0.71	0.009

Supporting Information captions

Fig. S1 SEM images of (a-c) the dry banana peel precursor (BP) and (d-f) banana peel derived char (BP-char) pyrolysed at 873 K for 1 hour.

Fig. S2 EDX analysis of (a) BPC- (b) BPC-1023-Ar-3h (c) BPC-1273-Ar-3h.

Table S 1 Measured absolute adsorption capacities for CO₂, CH₄, and N₂ on BPC-1273-CO₂-1h at 298 K, 313 K and 323 K, and the corresponding uncertainty $u(Q_{abs})$.

Table S 2 Measured absolute adsorption capacities for CO₂, CH₄, and N₂ on BPC-1273-Ar-3h at 298 K measured with the Belsorb-BG.